nature geoscience

LETTERS

PUBLISHED ONLINE: 3 AUGUST 2014 | DOI: 10.1038/NGEO2213

Stabilization of the coupled oxygen and phosphorus cycles by the evolution of bioturbation

R. A. Boyle[1,2*], T. W. Dahl[1,3], A. W. Dale[4], G. A. Shields-Zhou[5], M. Zhu[6], M. D. Brasier[7], D. E. Canfield[1] and T. M. Lenton[2]

Animal burrowing and sediment-mixing (bioturbation) began during the run up to the Ediacaran/Cambrian boundary[1–3], initiating a transition[4,5] between the stratified Precambrian[6] and more well-mixed Phanerozoic[7] sedimentary records, against the backdrop of a variable[8,9] global oxygen reservoir probably smaller in size than present[10,11]. Phosphorus is the long-term[12] limiting nutrient for oxygen production via burial of organic carbon[13], and its retention (relative to carbon) within organic matter in marine sediments is enhanced by bioturbation[14–18]. Here we explore the biogeochemical implications of a bioturbation-induced organic phosphorus sink in a simple model. We show that increased bioturbation robustly triggers a net decrease in the size of the global oxygen reservoir—the magnitude of which is contingent upon the prescribed difference in carbon to phosphorus ratios between bioturbated and laminated sediments. Bioturbation also reduces steady-state marine phosphate levels, but this effect is offset by the decline in iron-adsorbed phosphate burial that results from a decrease in oxygen concentrations. The introduction of oxygen-sensitive bioturbation to dynamical model runs is sufficient to trigger a negative feedback loop: the intensity of bioturbation is limited by the oxygen decrease it initially causes. The onset of this feedback is consistent with redox variations observed during the early Cambrian rise of bioturbation, leading us to suggest that bioturbation helped to regulate early oxygen and phosphorus cycles.

The first widely accepted trace fossil evidence for locomotion at about 565 million years ago (Ma; ref. 1) is succeeded by very shallow, three-dimensional burrowing from about 555 Ma (refs 2,3). This is followed by an increase in the diversity of observable bioturbation traces across the Ediacaran/Cambrian boundary[19]; from around 540 Ma burrows tend to appear in more inshore environments, and become larger and more frequently open-ended[19,20]. An emerging view of this early Cambrian 'substrate revolution' suggests largely unmixed sediments in some parts of the continental shelf[5], during what was presumably a spatially heterogeneous ocean sediment system, undergoing a transitional phase involving progressive loss of sediment stratification. Nevertheless, it is clear that by ~530–525 Ma the intensity of bioturbation had increased significantly[3]. Between Cambrian Stages 1 (541 to ~529 Ma) and 2 (~529 to ~521 Ma), maximum burrow depths rose to almost modern levels of up to a metre, and the bioturbation index (a measure of the percentage of primary bedding fabric disrupted by bioturbation[21]) changed from 0.5 to 2.3 (ref. 3), a value around which it remained around until Cambrian Stage 5.

The palaeoredox context in which this biological change occurred is depicted in Fig. 1, which shows a compilation of U and Mo concentration and Mo isotope data[10] alongside the average and maximum bioturbation index[3,21] between 580 and 490 Ma. Between approximately 520 and 510 Ma, after the initial increase in the average bioturbation index, marine shale δ^{98}Mo, U and Mo content points to declining oxygen, over a time interval of around 10–15 million years. We argue this is consistent with a decrease in the size of the global oxygen reservoir immediately after the first appreciable bioturbation. It is important to emphasize the need for caution in any attempt at a quantitative reconstruction of the trajectory of the global oxygen reservoir during this time interval, and that temporal variability is implied by existing data. For example, some data from ~499 Ma point to widespread euxinia[11], although, conversely, a pulse of oxygenation has also been suggested 1–2 million years later[22]. Nevertheless the δ^{98}Mo proxy does specifically focus on reservoir size changes[10], and does imply declining oxygen.

The earliest moving animals would, of course, have required organic carbon for food, which today is predominantly buried in continental shelf sediments[23]. Within such sediments bioturbation would have reduced stratification, and bioirrigation would have increased the reactive surface area for chemical exchange with the water column. The potential significance of the impact of these sorts of changes on sediment composition is illustrated by the behaviour of phosphorus. Marine shales derived from bioturbated sediments exhibit organic C:P ratios as low as 150, whereas those derived from laminated sediments can have C:P ratios of up to 3,900 (ref. 15), with typical values in the region of 500–700 (refs 16,24). There are three probable mechanisms[14,15] responsible for these differences: (1) microbial polyphosphate sequestration in well-mixed sediments under oxygenated conditions[14,18], with subsequent accumulation of refractory organic P compounds; (2) greater retention of phosphate via adsorption on Fe oxyhydroxides[14,15] in sediments exposed to oxygenated waters by bioturbation (leading to subsequent P burial in inorganic phases); (3) enhanced organic carbon preservation in anoxic and/or euxinic conditions[14] (that is, aside from any change in P), due ultimately to the increased energy yield of aerobic respiration.

These mechanisms are already represented in existing models of the long-term coupling between the phosphorus and oxygen cycles, but redox-linked changes in modelled C:P ratios of buried

[1]Institute of Biology and Nordic Centre for Earth Evolution, University of Southern Denmark, Campusvej 55, 5230 Odense M, Odense, Denmark, [2]Laver Building, College of Life and Environmental Sciences, University of Exeter, North Park Road, Exeter EX4 4QE, UK, [3]Natural History Museum of Denmark, University of Copenhagen, Øster Voldgade 5-7, 1350 København K, Denmark, [4]GEOMAR Helmholtz Centre for Ocean Research Kiel, Wischhofstrasse 1-3, 24148 Kiel, Germany, [5]Department of Earth Sciences, University College London, Gower Street, London WC1E 6BT, UK, [6]Nanjing Institute of Geology and Palaeontology, Chinese Academy of Sciences, 39 East Beijing Road, Nanjing 210008, China, [7]Department of Earth Sciences, University of Oxford, South Parks Road, Oxford OX1 3AN, UK. *e-mail: rboyle@biology.sdu.dk

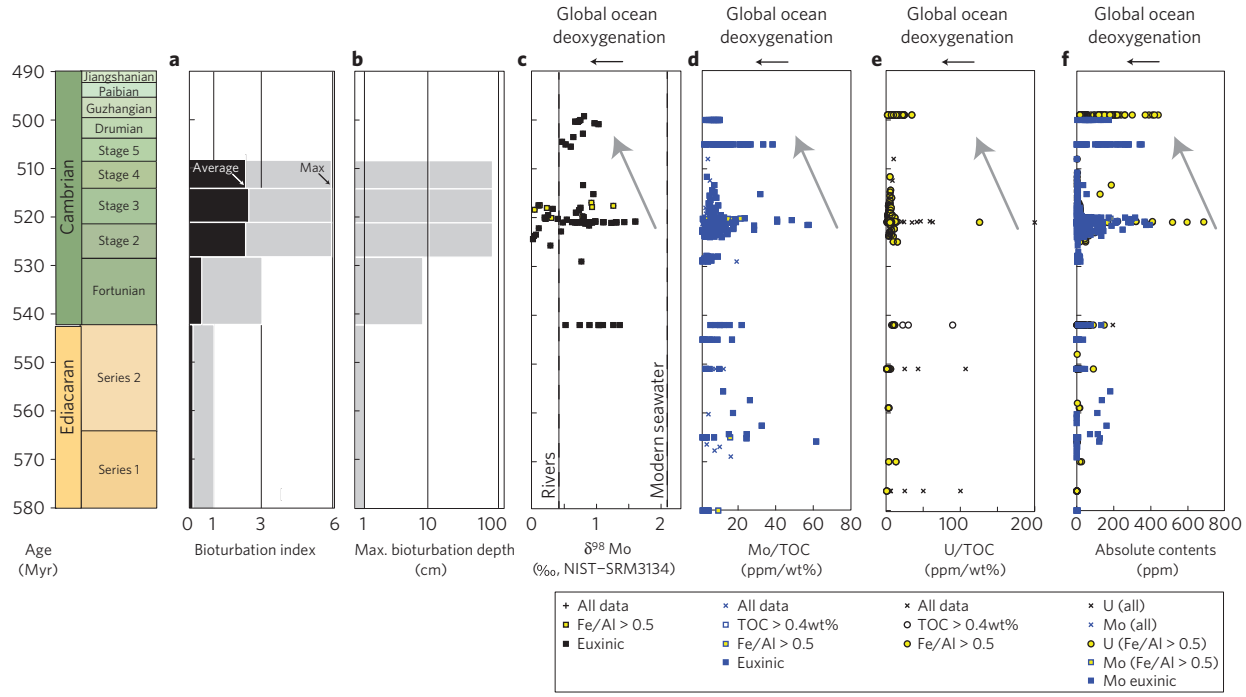

Figure 1 | Redox proxy data is consistent with decreased oxygenation of the marine environment following the early Cambrian increase in bioturbation. a,**b**, Bioturbation data from ref. 3. Bioturbation index[3,22] refers to the percentage of the original sediment fabric exhibiting disturbance by bioturbation: 0 = 0%, 1 = 1–4%, 2 = 5–30%, 3 = 31–60%, 4 = 61–90%, 5 = 91–99%, 6 = 100%. **c**, Molybdenum isotope compositions $\delta^{98}Mo = [(^{98}Mo/^{95}Mo)_{sample}/(^{98}Mo/^{95}Mo)_{NIST-SRM3134} - 1] \cdot 1{,}000$ [‰]. Seawater $\delta^{98}Mo$ scales positively with ocean oxygenation. The maximum $\delta^{98}Mo$ value (rather than the mean) is the strongest indicator of the extent of ocean oxygenation, because mildly euxinic shales have a lower $\delta^{98}Mo$ than ambient seawater. **d**–**f**, Mo/TOC (**d**), U/TOC (**e**) and sedimentary Mo and U contents (**f**). Both Mo and U are soluble in oxic waters and more efficiently removed under anoxic and sulphidic conditions. Normalization to TOC scales out the dependence of trace metal enrichment on TOC content. Anoxic settings identified by Fe:Al > 0.5, euxinic settings by $Fe_{(highly\ reactive/total)} > 0.38$ and $Fe_{(pyritized/highly\ reactive)} > 0.7$ (see Supplementary Table 3 for further details and full references). Arrows mark intervals of the proposed relative oxygen decline.

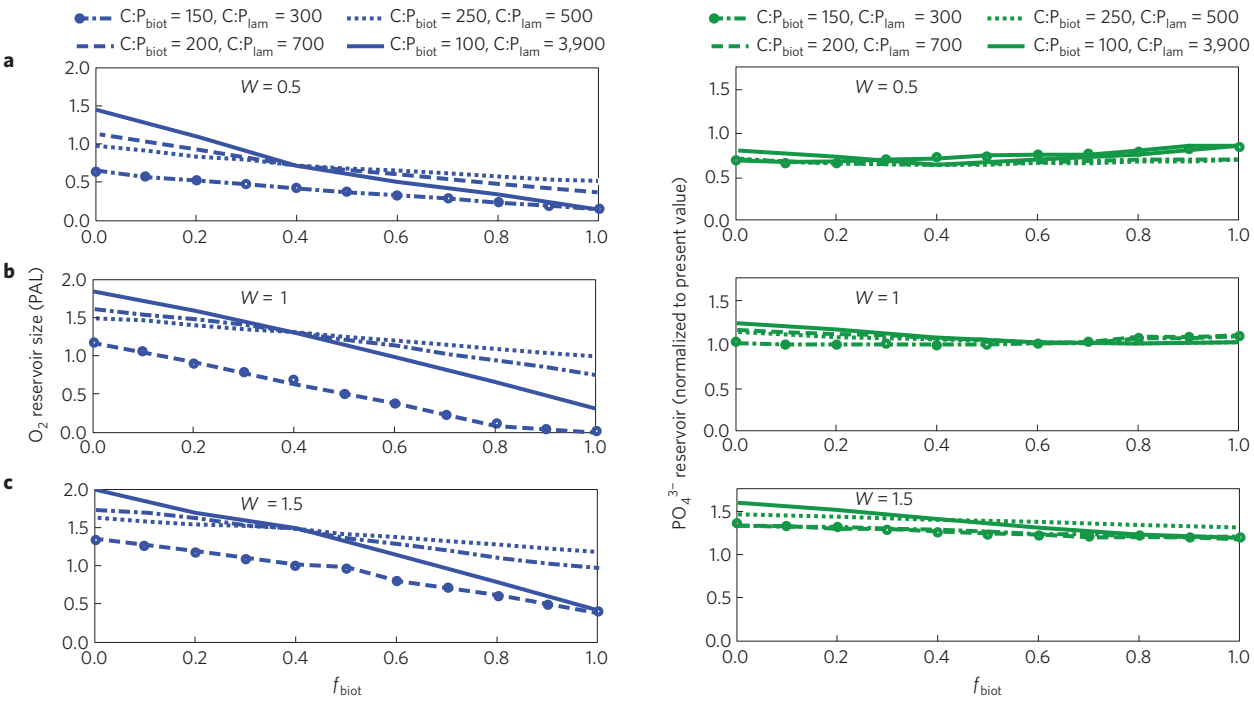

Figure 2 | Modelled steady-state oxygen/phosphorus reservoir sizes as a function of bioturbation. Steady-state size of the atmosphere/surface oxygen (blue, left) and marine phosphorus (green, right) reservoirs for different bulk weathering forcings $W = 0.5$ (**a**), $W = 1.0$ (**b**), $W = 1.5$ (**c**) relative to the present and with different values for the organic carbon to phosphorus ratio for bioturbated $C:P_{biot}$ and laminated $C:P_{lam}$ sediments (as indicated by the different linestyles on each plot).

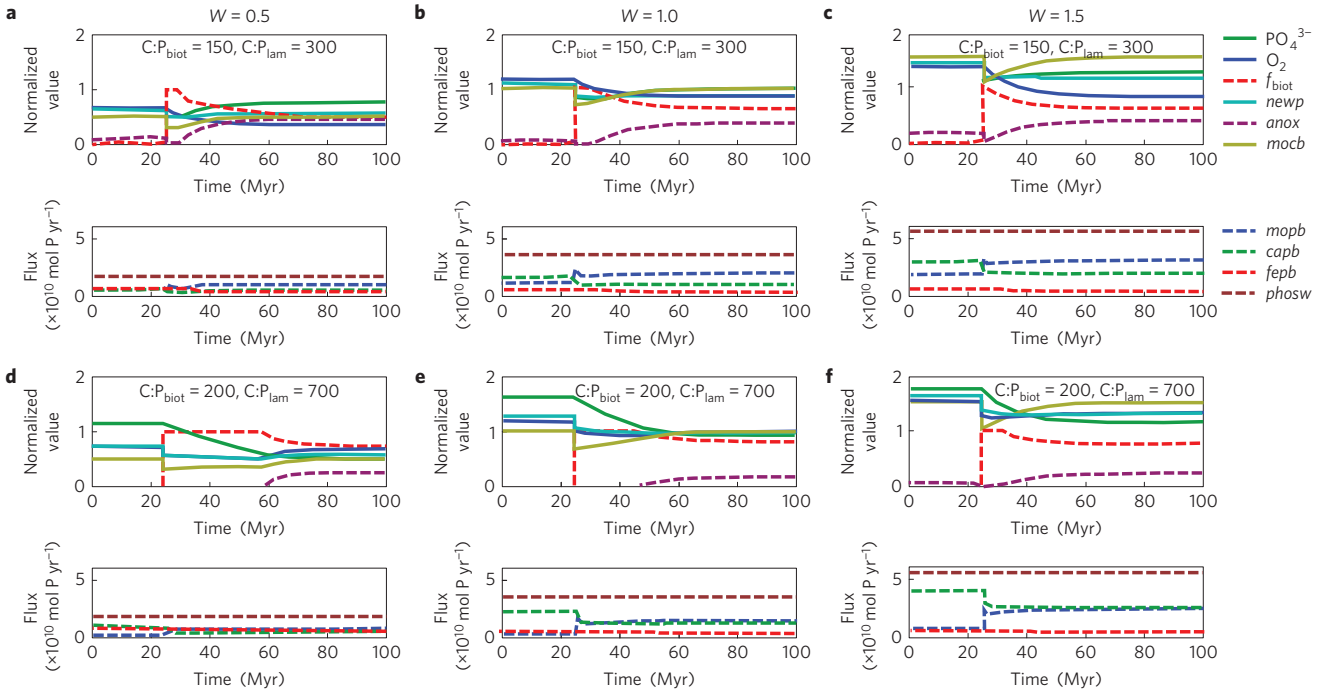

Figure 3 | Examples of the dynamic model response to the introduction of oxygen-sensitive bioturbation. Model initialized at a steady state with negligible bioturbation, $f_{biot} = 0.01$, then dynamic bioturbation $f_{biot} = 1 - anox$ (where *anox* is the ocean anoxic fraction) is introduced 25 million years into each 100-million-year simulation. For each model run the upper panel in the subfigure shows the marine reservoirs (relative to their modern values) and relevant fluxes, while the lower panel in the subfigure shows the fluxes affecting the phosphorus reservoir (in absolute values of 10^{10} mol yr^{-1}). **a**–**c**, Moderate difference in prescribed C:P burial ratios $C{:}P_{biot} = 150$, $C{:}P_{lam} = 300$. **d**–**f**, Larger difference in prescribed C:P burial ratios $C{:}P_{biot} = 200$, $C{:}P_{lam} = 700$. Columns show different bulk weathering values $W = 0.5$ (**a**,**d**), $W = 1.0$ (**b**,**e**), $W = 1.5$ (**c**,**f**). Abbreviations: PO_4, marine phosphate reservoir; O_2, atmosphere/surface ocean oxygen reservoir; f_{biot}, bioturbated fraction of buried organic matter; *newp*, new production; *anox*, ocean anoxic fraction; *mocb*, marine organic carbon burial; *mopb*, marine organic phosphorus burial; *capb*, calcium-bound phosphate burial; *fepb*, iron adsorbed phosphate burial; *phosw*, phosphorus weathering.

organic matter are expressed as a function of the ocean anoxic fraction, rather than bioturbation[25,26]. In this work, we focus on the timing of the onset of the sensitivity of organic phosphorus burial to ocean oxygenation, making the case that this sensitivity can be attributed to bioturbation. We hypothesize that increased exposure of sediments to oxygen in overlying water, caused by bioturbation and bioirrigation, initiated an organic phosphorus sink through increased microbial polyphosphate sequestration[18] (that is, mechanism (1)) for the first time during the early Cambrian.

We adapted an existing model[26] (Methods), describing the coupled long-term dynamics of the marine phosphate and nitrate reservoirs, and the oxygen content of the atmosphere (and surface ocean). The model includes a weak inverse dependence of organic carbon burial on water column O_2 (ref. 13; mechanism (3)), as well as the removal of phosphate with ferric iron (Fe^{3+}) oxyhydroxides[25], which ceases under anoxic conditions (mechanism (2)). The burial flux of marine organic phosphorus *mopb* is related to that of marine organic carbon *mocb* through the bioturbated fraction f_{biot} of buried organic matter, which dictates the apportioning between the low burial ratio $C{:}P_{biot}$ of bioturbated sediments, and the higher value of laminated sediments $C{:}P_{lam}$:

$$mopb = mocb \cdot \left(\frac{f_{biot}}{C{:}P_{biot}} + \frac{1 - f_{biot}}{C{:}P_{lam}} \right) \quad (1)$$

Mathematically this is a very simple modification to existing models, but conceptually speaking we suggest that bioturbation is more important in determining sedimentary organic C:P burial ratios than the oxygenation state of the overlying water per se. For example, sediments intermittently oxygenated by bioturbation exhibit C:P ratios closer to permanently oxygenated sediments than to anoxic sediments[17], whereas even under an oxygenated water column an undisturbed sediment will become anoxic within approximately 2.5 cm of the sediment–water interface[27]. Furthermore, we suggest that even incompletely mixed sediments would have undergone an increase in propensity to support microbial P sequestration through increased bioirrigation.

Our central result is depicted by the steady-state solutions shown in Fig. 2. Increasing the bioturbated fraction f_{biot} of buried organic matter leads to a reduction in the size of the global oxygen reservoir—across the range of potential C:P burial ratios for bioturbated and laminated sediments, and across various different bulk weathering rates. This is because increased marine organic phosphorus burial results from increasing f_{biot}. The feedback sequence giving rise to this result is illustrated in Fig. 3, which shows example dynamical runs in which we ran the model to steady state with negligible bioturbation ($f_{biot} = 0.01$), before introducing oxygen sensitive bioturbation $f_{biot} = 1 - anox$ (where *anox* is the anoxic fraction of ocean waters (Methods)). Bioturbation leads to increased marine organic phosphorus burial, decreasing (phosphorus-limited) new production, marine organic carbon burial, and oxygen. As oxygen drops and anoxia increases, organic carbon burial increases due to reduced remineralization. Increased anoxia also weakens the Fe-oxyhydroxide phosphate sink, causing a secondary increase in phosphate (and, therefore, new production and organic carbon burial). This compensating increase in phosphate as anoxia rises explains why the impact of increased f_{biot} on the phosphate reservoir is weaker than the impact on oxygen.

The differing response of the phosphate reservoir to that of oxygen is also affected by how close the system is to anoxia before

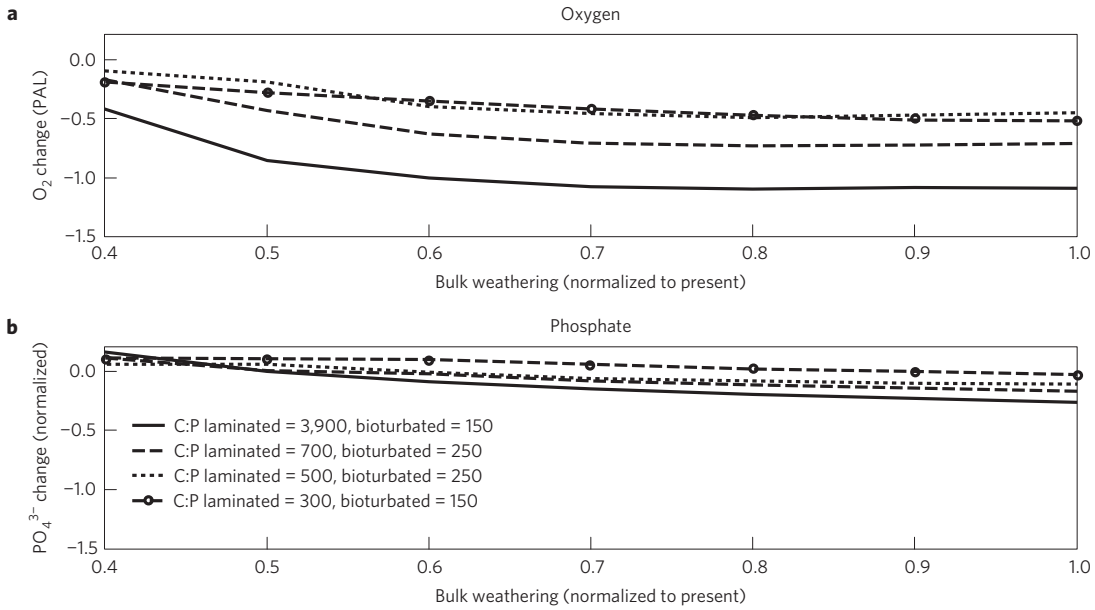

Figure 4 | Net change in steady-state oxygen and phosphate reservoirs due to the introduction of dynamical oxygen-sensitive bioturbation. The model was allowed to reach steady state with negligible bioturbation, then dynamical bioturbation was introduced leading to a new steady state (that is, every point in Fig. 4 corresponds to a dynamical run equivalent to Fig. 3). Pre-bioturbation reservoir sizes were subtracted from their respective post-bioturbation values and the difference is expressed relative to the present-day reservoir size—that is, $(O_{2(after)} - O_{2(before)})/O_{2_0}$ and $(PO_{4(after)} - PO_{4(before)})/PO_{4_0}$. Results are shown as a function of bulk weathering rate (*x*-axis) with different C:P burial ratio parameter choices (as indicated by the linestyles in the legend). **a**, Change in atmosphere–surface–ocean oxygen reservoir. **b**, Change in marine phosphate reservoir.

the introduction of bioturbation. With low weathering $W = 0.5$ relative to the present, the lower initial oxygen reservoir size means that the bioturbation-induced phosphate sink more easily increases anoxia, feeding back negatively on the Fe–P burial flux early in the simulation, and leading to the (counter-intuitive) slight net increase in deep-ocean phosphate concentration. At higher weathering rates, the initial larger O_2 reservoir means a greater initial phosphate/oxygen decrease is necessary to induce anoxia, and the overall impact on the phosphate reservoir at steady state is a negative one.

The oxygen-sensitivity of bioturbation used in the dynamical runs (Fig. 3) causes f_{biot} to decline asymptotically owing to the drop in oxygen that it initially causes, and the resultant decrease in the organic phosphate burial flux helps the system approach a new, lower steady-state oxygen level (see also Supplementary Fig. 1). This qualitative feedback sequence is robust to changes in bulk weathering, the introduction of alternative formulations for oxidative weathering and organic carbon burial (Supplementary Figs 2 and 3), increased C:P ratio differences (Supplementary Fig. 4), and expression of f_{biot} as a direct increasing function of the global oxygen reservoir (Supplementary Fig. 5; as opposed to a decreasing function of anoxia). The key point that we wish to emphasize here is that the introduction of this feedback to the Earth system occurred as a consequence of the spread of the first bioturbating animals.

Quantitative thresholds on the overall change in the global oxygen and phosphate reservoirs potentially resulting from the introduction of bioturbation were assessed by comparing pre- and post-bioturbation steady states across a range of simulations. Figure 4 depicts the difference between the steady states with negligible bioturbation ($f_{biot} = 0.01$) and anoxia-sensitive bioturbation ($f_{biot} = 1 - anox$), for various C:P ratio and weathering parameters. The magnitude of the decline in the oxygen reservoir scales with the difference in C:P ratios between bioturbated and laminated sediments (also see Supplementary Fig. 4). The size of the change in atmospheric oxygen also increases with the weathering flux of phosphorus (up to ~70% of the present flux), above which anoxia (due to high productivity, rather than low oxygen, see Methods) leads to loss of Fe–P burial, limiting the potential change in phosphate that can be induced by the bioturbation-driven organic P sink.

The nature and stability of the pre-bioturbation oxygen/phosphorus steady state is an important outstanding uncertainty. A steady state with negligible bioturbation and weaker phosphate removal (that is, higher $C:P_{lam}$ within the pre-bioturbation organic phosphorus burial flux $mopb \approx mocb/CP_{lam}$) entails higher oxygen, but must nevertheless remain consistent with data for appreciable anoxia[11], implying that the organic phosphorus sink cannot have been too weak, even before the onset of bioturbation (this constraint is formalized analytically in the Supplementary Methods). This implies one of the following three alternatives: (1) atmospheric oxygen remained below present levels through the latest Neoproterozoic (with inorganic P-burial changes compensating for a high $C:P_{lam}$, keeping oxygen low); (2) there was sufficient organic P-scavenging even before bioturbation to adequately reduce $C:P_{lam}$ such that it was toward the lower end of modern observations; (3) widespread anoxic conditions ceased with the Neoproterozoic oxygenation event (or at least were more restricted than present), only recurring much later. Intriguingly, the final possibility would imply weak to negligible regulation of the oxygen reservoir (at least by ocean biogeochemistry) before the rise of bioturbation.

Some form of qualitative reorganization of the global phosphorus cycle is broadly consistent with phosphorite deposition across the Precambrian/Cambrian boundary[28], perhaps linked to increased anaerobic remineralization connected to a bioturbation-induced oxygen decline (Supplementary Fig. 6). However, substantial phosphorite deposition occurs well before the onset of bioturbation[28], so bioturbation cannot provide a comprehensive explanation for this phenomenon. A bioturbation-driven organic phosphorus sink is also potentially consistent with the downward trajectory of C:P ratios around 500 Ma (ref. 29), although more data is needed for the earlier Cambrian to test this supposition. Most directly, the data we present in Fig. 1 shows how, after the initial increase in bioturbation

intensity during Cambrian Stage 2, trace element burial and isotopic trends are consistent with a drop in ocean oxygenation and a relative decrease in the size of the global oxygen reservoir.

Our results thus suggest that the earliest bioturbating animals caused a relative decline in the size of the oxygen reservoir on which they depended, initiating a net negative feedback loop through the creation of an oxygen-sensitive phosphorus sink. This strengthened the link between the oxygen and phosphorus biogeochemical cycles, and contributed to oxygen regulation across Phanerozoic time.

Methods

Redox-sensitive trace element data. Molybdenum is soluble as the molybdate MoO_4^{2-} anion in oxygenated conditions, which is removed slowly via adsorption onto Mn oxides. In sulphidic solutions, molybdate reacts with H_2S to form reactive oxythiomolybdates $MoO_{4-x}S_x^{2-}$, which are reductively removed from solution. Distinct isotopic fractionation and burial rates are associated with fully oxygenated waters, low oxygen non-euxinic settings that become sulphidic at depth and fully euxinic settings. All these sinks preferentially remove ^{95}Mo, but the strongest fractionation is associated with oxic settings, so that increasing seawater δ^{98}Mo indicates increasing ocean oxygenation. Because the δ^{98}Mo of euxinic shales can be lower than that of seawater, the maximum δ^{98}Mo value in shales (rather than the mean) is generally the most reliable indicator of the Mo isotopic composition of the oceans in which they were deposited. This maximum value is set by the fraction of ocean sediments that are fully oxygenated (because these oxygenated settings impart the strongest fractionation). Because the residence time of Mo (today ~400 kyr) is much longer than the mixing time of the Earth's oceans (~1.5 kyr), seawater is well-mixed and homogeneous with respect to Mo. Similarly, uranium a has a soluble oxidized state (hexavalent U(VI), stable in oxygenated water as uranyl tetracarbonate $UO_2(CO_3)_3^{4-}$) and an immobile reduced state (tetravalent U(IV), readily sequestered into organic rich shales in low oxygen conditions). Figure 1 shows the U concentration in shales, relative to total organic carbon (which will positively correlate with ambient seawater U concentration and, thus, ocean oxygenation). See, for example, refs 10,30 for detailed considerations of ancient ocean oxygenation in relation to Mo and U, respectively. We argue that the fact that a downward trajectory in ocean oxygenation is implicit in two distinct trace elements lends weight to the possibility of a net oxygen decrease in conjunction with the rise of bioturbation.

Model. The 'Redfield revisited' model of ref. 26 (incorporating key phosphorus cycle functions from ref. 25) describes the change over time in the size of the global phosphorus PO_4 nitrate NO_3 and oxygen O_2 reservoirs (see also feedback diagram in Supplementary Fig. 7):

$$\frac{dPO_4}{dt} = phosw - fepb - capb - mopb$$

$$\frac{dNO_3}{dt} = nfix - monb - denif$$

$$\frac{dO_2}{dt} = mocb - oxidw$$

Normalization and reservoir size/concentration scaling. The total size (in moles) of the above three reservoirs is assumed to scale linearly with the average concentration (in mol kg^{-1} seawater) in marine surface waters ventilating the deep ocean, via scaling factors[26] $k_{N,P} = 7.1 \times 10^{-22}$ kg^{-1} and $k_O = 8.96 \times 10^{-24}$ kg^{-1}. Thus, concentrations in moles per kilogram seawater are $O_{2CONC} = O_2 \cdot k_O$, $NO_{3CONC} = NO_3 \cdot k_{N,P}$ and $PO_{4CONC} = PO_4 \cdot k_{N,P}$. Present day average surface water concentrations used for normalization are $O_{2CONC0} = 331.5 \times 10^{-6}$ mol kg^{-1}, $NO_{3CONC0} = 30.9 \times 10^{-6}$ mol kg^{-1}, $PO_{4CONC0} = 2.2 \times 10^{-6}$ mol kg^{-1}, in moles per kilogram of seawater. Where normalized concentrations are used (denoted by an overscore) we therefore have $\overline{O_{2CONC}} = O_{2CONC}/O_{2CONC0}$, $\overline{NO_{3CONC}} = NO_{3CONC}/NO_{3CONC0}$ and $\overline{PO_{4CONC}} = PO_{4CONC}/PO_{4CONC0}$. When normalized, reservoir sizes are referred to this is relative to present day values (in moles) of $O_{2_0} = 3.7 \times 10^{19}$, $NO_{3_0} = 4.35 \times 10^{16}$ and $PO_{4_0} = 3.1 \times 10^{15}$.

Fluxes. Default values for fluxes and parameters are given in Supplementary Tables 1 and 2. W denotes the bulk weathering forcing relative to present. Fluxes are in units of moles per year and the zero subscript denotes present day value. Phosphorus is added to the ocean via phosphorus weathering $phosw = W \cdot phosw_0$ and removed by iron-adsorbed phosphate burial $fepb = fepb_0((1-anox)/k_{ox})$, where the anoxic fraction is $anox = MAX(0, 1 - k_{ox} \cdot \overline{O_{2CONC}}(newp_0/newp))$, $k_{ox} = 0.86$ is the present day ocean's oxic fraction and new production $newp = newp_0 \cdot MIN(117PO_{4CONC}, (117/16)NO_{3CONC})$ in units of moles organic carbon per kilogram seawater, scales stoichiometrically with limiting nutrient concentration. Phosphorus also leaves the marine reservoir through calcium bound phosphate burial $capb = capb_0 \cdot (newp/newp_0)^2$ and marine organic phosphorus burial $mopb = mocb \cdot (f_{biot}/C{:}P_{biot} + (1-f_{biot})/C{:}P_{lam})$. Nitrate changes via nitrogen fixation

$$nfix = MAX\left(0, nfix_0 \cdot \left(\frac{PO_{4CONC} - \frac{NO_{3CONC}}{16}}{\left(PO_{4CONC0} - \frac{NO_{3CONC0}}{16}\right)}\right)\right)$$

(when nitrate is deficient relative to Redfield stoichiometry with phosphate), marine organic nitrogen burial $monb = mocb/37.5$ and denitrification $denif = denif_0 \cdot (1 + (anox/anox_0))$, but is not directly relevant to the results discussed in this paper, beyond supporting the assumption that phosphorus is limiting over long timescales. Marine organic carbon burial $mocb = mocb_0 \cdot (newp/newp_0)^2 \cdot De^{-BO_{2CONC}}$ (with $D = 2.127$, $B = 2{,}277$ mol^{-1} kg) adds to the oxygen reservoir and oxidative weathering $oxidw = oxidw_0 W$ removes from it.

This work differs from the original model by the use of equation (1) in the main text and, for Figs 3 and 4, by putting $f_{biot} = 1 - anox$. The model was numerically integrated in Matlab using a Runge–Kutta solver. For more detailed model description, see Supplementary Methods. Analytic solutions show how simultaneous non-zero steady-state oxygen and anoxia impose constraints on the scaling factor used to relate marine organic carbon and phosphorus burial:

$$\frac{phosw_0 - \frac{fepb_0}{k_{ox} \cdot W} - \frac{capb_0}{f_{remin}}}{oxidw_0} \leq \frac{f_{biot}}{C{:}P_{biot}} + \frac{1-f_{biot}}{C{:}P_{lam}} < \frac{phosw_0 - \frac{capb_0}{f_{remin}}}{oxidw_0}$$

which can be rearranged to give maximum and minimum values for f_{biot} in terms of the C:P burial ratios, or (for a pre-bioturbation ocean) constrain the strength of the phosphorus sink in terms of $C{:}P_{lam}$. We also find that the partial derivative of steady-state normalized oxygen with respect to the bioturbated fraction is always less than zero:

$$\frac{\partial \overline{O_{2CONC}}}{\partial f_{biot}} = -\frac{W^{\frac{3}{2}} \cdot mocb_0}{fepb_0 \sqrt{f_{remin}}} \left(\frac{1}{C{:}P_{biot}} - \frac{1}{C{:}P_{lam}}\right) < 0$$

supporting the basic result. Default flux values and a derivation of the analytic results are given in the Supplementary Methods.

Received 14 May 2014; accepted 30 June 2014; published online 3 August 2014

References

1. Liu, A. G., McIlroy, D. & Brasier, M. D. First evidence for locomotion in the Ediacara biota from the 565 Ma Mistaken Point Formation, Newfoundland. *Geology* **38,** 123–126 (2010).
2. Menon, L., McIlroy, D. & Brasier, M. D. Evidence for Cnidaria-like behavior in ca. 560 Ma Ediacaran *Aspidella*. *Geology* **41,** 895–898 (2013).
3. Mangano, M & Buatois, L. A. Decoupling of body plan diversification and ecological structuring during the Ediacaran–Cambrian transition: Evolutionary and geobiological feedbacks. *Proc. R. Soc. B* **281,** 20140038 (2014).
4. Buatois, L. A., Narbonne, G. M., Mangano, M. G., Carmona, M. B. & Myrow, P. Ediacaran matground persisted into the earliest Cambrian. *Nature Commun.* **5,** 3544 (2014).
5. Tarhan, L. G. & Droser, M. L. Widespread delayed mixing in early to middle Cambrian marine shelfal settings. *Palaeogeogr. Palaeoclimatol. Palaeoecol.* **399,** 310–322 (2014).
6. Seilacher, A. Biomat-related lifestyles in the Precambrian. *Palaios* **14,** 86–93 (1999).
7. Droser, M. L. & Bottjer, D. J. Trends and patterns of Phanerozoic ichnofabrics. *Ann. Rev. Earth Planet. Sci. Lett.* **21,** 205–225 (1993).
8. Frei, R., Gaucher, C., Poulton, S. W. & Canfield, D. E. Fluctuations in Precambrian atmospheric oxygenation recorded by chromium isotopes. *Nature* **461,** 250–254 (2009).
9. Scott, C. *et al.* Tracing the stepwise oxidation of the Proterozoic ocean. *Nature* **452,** 456–460 (2008).
10. Dahl, T. W. *et al.* Devonian rise in atmospheric oxygen correlated to the radiations in terrestrial plants and large predatory fish. *Proc. Natl Acad. Sci. USA* **107,** 17911–17915 (2010).
11. Gill, B. C. *et al.* Geochemical evidence for widespread euxinia in the later Cambrian ocean. *Nature* **469,** 80–83 (2011).

12. Redfield, A. C. The biological control of chemical factors in the environment. *Am. Sci.* **46,** 205–221 (1958).
13. Betts, J. N. & Holland, H. D. The oxygen content of ocean bottom waters, the burial efficiency of organic carbon, and the regulation of atmospheric oxygen. *Palaeogeogr. Palaeoclimatol. Palaeoecol.* **97,** 5–18 (1991).
14. Ingall, E. & Jahnke, R. Evidence for enhanced phosphorus regeneration from marine sediments overlain by oxygen depleted waters. *Geochim. Cosmochim. Acta* **58,** 2571–2575 (1994).
15. Ingall, E. D., Bustin, R. M. & Van Cappellen, P. Influence of water column anoxia on the burial and preservation of carbon and phosphorus in marine shales. *Geochim. Cosmochim. Acta* **57,** 303–316 (1993).
16. Anderson, L. D., Delaney, M. L. & Faul, K. L. Carbon to phosphorus ratios in sediments: Implications for nutrient cycling. *Glob. Biogeochem. Cycles* **15,** 65–79 (2001).
17. Aller, R. C. Bioturbation and remineralization of sedimentary organic matter: Effects of redox oscillation. *Chem. Geol.* **114,** 331–345 (1994).
18. Kerrn-Jespersen, J. P. & Henze, M. Biological phosphorus uptake under anoxic and aerobic conditions. *Water Res.* **27,** 617–624 (1993).
19. Droser, M. L. & Bottjer, D. J. Trends in depth and extent of bioturbation in Cambrian carbonate marine environments, western United States. *Geology* **16,** 233–236 (1988).
20. McIlroy, D. & Logan, G. A. The impact of bioturbation on infaunal ecology and evolution during the Proterozoic–Cambrian transition. *Palaios* **14,** 58–72 (1999).
21. Taylor, A., Goldring, R. & Gowland, S. Analysis and application of ichnofabrics. *Earth Sci. Rev.* **60,** 227–259 (2003).
22. Saltzman, M. R. *et al.* Pulse of atmospheric oxygen during the late Cambrian. *Proc. Natl Acad. Sci. USA* **108,** 3876–3881 (2011).
23. Berner, R. A. Burial of organic carbon and pyrite sulphur in the modern ocean: Its Geochemical and environmental significance. *Am. J. Sci.* **282,** 451–473 (1982).
24. Slomp, C. P., Thomson, J. & de Lange, G. J. Controls on phosphorus regeneration and burial during formation of eastern Mediterranean sapropels. *Mar. Geol.* **203,** 141–159 (2004).
25. Van Cappellen, P. & Ingall, E. D. Benthic phosphorus regeneration, net primary production, and ocean anoxia: A model of the coupled marine biogeochemical cycles of carbon and phosphorus. *Paleoceanography* **9,** 677–692 (1994).
26. Lenton, T. M. & Watson, A. J. Redfield revisited: 2. What regulates the oxygen content of the atmosphere? *Glob. Biogeochem. Cycles* **14,** 249–268 (2000).
27. Gundersen, J. K. & Jorgensen, B. B. Microstructure of diffusive boundary layers and the oxygen uptake of the seafloor. *Nature* **345,** 604–607 (1993).
28. Papineau, D. Global biogeochemical changes at both ends of the proterozoic: Insights from phosphorites. *Astrobiology* **10,** 165–181 (2010).
29. Algeo, T. J. & Ingall, E. Sedimentary C_{org}:P ratios, paleocean ventilation, and Phanerozoic atmospheric pO_2. *Palaeogeogr. Palaeoclimatol. Palaeoecol.* **256,** 130–155 (2007).
30. Partin, C. A. *et al.* Large scale fluctuations in Precambrian atmospheric and oceanic oxygen levels from the record of U in shales. *Earth. Plan. Sci. Lett.* **369–370,** 284–293 (2013).

Acknowledgements

R.A.B., T.M.L. and G.A.S-Z. gratefully acknowledge funding from the National Environment Research Council (NE/I005978/1). T.W.D. was sponsored from the Inge Lehmann Scholarship and the VILLUM Foundation (VKR023127). M.Z. is funded by the National Basic Research Program of China (2013CB835000) and the National Natural Science Foundation of China (40930211). A.W.D. was supported by the SFB754, funded by the German DFG (www.sfb754.de).

Author contributions

R.A.B., T.M.L., G.A.S-Z. and M.Z. developed the hypothesis, including ideas from all co-authors. T.W.D. provided data. R.A.B. modified the original model of T.M.L. R.A.B. wrote the paper with input from all co-authors.

Additional information

Supplementary information is available in the online version of the paper. Reprints and permissions information is available online at www.nature.com/reprints. Correspondence and requests for materials should be addressed to R.A.B.

Competing financial interests

The authors declare no competing financial interests.